Amphibious Rescue Vessel Based on Planetary Rotating Paddled Wheel

Haokun Xie *

Tabor Academy, MA, USA

* Corresponding Author Email: kevinxie2026@163.com

Abstract. According to the 2021 World Trade Data, maritime transportation accounts for approximately 80% of global cargo transportation. However, with the increasing demand for trade, accidents at sea are also on the rise. When rescue personnel are dispatched to the scene for recovery, their lives are threatened due to the lack of good rescue ships, and there is an urgent need for amphibious rescue ships with fast speed and strong obstacle crossing capabilities through narrow spaces. Therefore, this project develops an amphibious rescue vessel to provide life support for rescue personnel. The amphibious rescue ship mainly consists of a hull and four inclined spoke paddles. When the wheels rotate, six paddles are rotated to change the driving force, thereby generating a combined force in the direction of the robot's movement and meeting the speed requirements during rescue. In terms of electronic design, Arduino nano, closed-loop stepper motor with FOC, voltage reduction module, and HC-12 are mainly used as hardware modules. The movement of the structure is achieved by driving the gear module and planetary reduction structure through the stepper motor. Driving tests were conducted in various environments including ground, water, and obstacle crossing, and it was found that the amphibious rescue ship performed excellently, meeting the practical requirements of fast speed and strong obstacle crossing ability.

Keywords: Paddle wheel, Amphibious, Rescue, ESP32.

1. Introduction

Ocean transportation, as an important means of national economic development, can obtain a large number of resources with the development of maritime industry. In addition, due to the advancement of shipbuilding technology, maritime trade has become an important mode of trade between continental plates. According to the 2021 World Trade Data, maritime transportation accounts for approximately 80% of global cargo transportation. However, with the increase of maritime activities, marine accidents have also correspondingly increased (Figure 1), which may be caused by human errors and organizational problems in management systems, or by ship engineering issues. No matter how advanced the future shipbuilding and navigation technology is, accidents will continue to occur. During the process of accident rescue, rescue personnel may face life-threatening situations due to the falling of goods, luggage, broken objects, and other items. In addition, due to the lack of obstacle crossing capability of existing rescue ships, it is difficult for rescue personnel to enter the disaster site. Therefore, a more superior amphibious rescue ship is a safer and more effective choice to replace rescue personnel in entering dangerous scenes [1]. In this context, develop an amphibious rescue vessel to assist in rescue operations in environments that are difficult for rescue personnel to enter or too dangerous.

Figure 1. Marine accidence.

AmphiHex-I is an amphibious hexapod robot [2] (Figure 2). The robot has 6 flip legs. When moving on land, the legs turn into an arc and drill into sand or soil to provide forward power. When transferring from land to water, the legs will stretch out and paddle at different angles to achieve different movements.

Figure 2. Amphibious hexapod robot.

Amphie II is an amphibious hexapod robot (as shown in Figure 3). The wheels of the robot consist of six fan-shaped frames, used for movement on land, and the middle blade is used for movement underwater. The robot uses a tripod gait to walk on land and flexible flippers to swim underwater. When swimming, six independent motors allow each leg to move independently. When moving underwater, rotate your legs back and forth by 60 degrees at different angles. By adjusting these actions, the robot can perform different maneuvers such as cruising, diving, surfacing, and turning. At the same time, robots can also achieve transitions from land to water and from water to land [3].

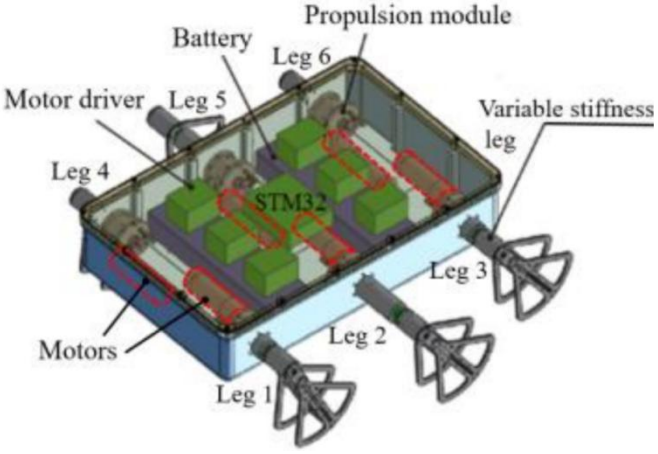

Figure 3. An amphibious robot with wheeled propeller legs.

Beyond hexapod designs, the academic literature has assessed a wide variety of locomotion approaches for amphibious robots. There has been a considerable focus on quadrupedal robots (those that have four legs), which mimic animal gaits to adjust to complex terrain [4], sometimes with inspiration from biology such as compliant footpads [5] or duck feet [6]. Other designs have been more niche, such as robots that walk on the seabed [7], robots which are designed to optimize walking on underwater principles [8], or visually guided swimming robots ([9]). The breadth of material provides a useful starting point to develop new rescue types of equipment, especially those characterized by high-speed performance across difficult surfaces [10].

2. Design

2.1. Structure design

2.1.1. Version 1

In this paper, we developed an amphibious robot to solve such problem. To achieve amphibious, the robot has four paddlewheels, adapting to both land environment and aquatic environment. When moving in aquatic environment, the planet gear in the wheels rotate the 6 paddles on all four wheels, making the paddle horizontal on top, and vertical on the bottom. The difference in paddle area provide momentum for the robot to move on land. When crossing obstacles, the paddles provide extra grip so that the robot can overcome bigger obstacle. Due to the paddlewheel, the robot does not require any additional transition module when transiting from land to water or from water to land, which allows the electronic components to be limited to only two motor and one chip. This greatly reduce the weight, cost of production, and greatly improves the compacity of the robot.

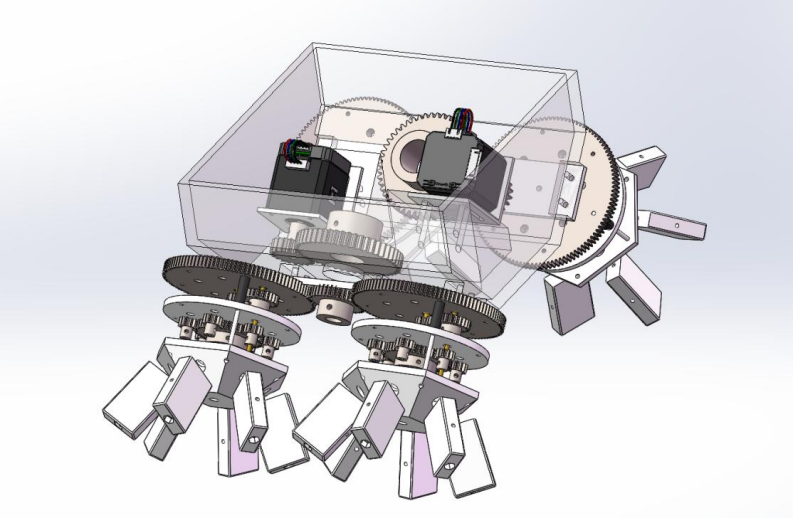

Figure 4. Amphibious paddle wheel vessel.

The vessel mainly consists of the hull and ASPW drive components as shown in Figure 4. The interior of the ship mainly includes the shell, motor bracket, main control module, power supply, switch, and voltage reduction module (supplementary). The ASPW drive part is mainly composed of cylindrical gears, supporting copper columns, and slurry. The hull is mainly responsible for buoyancy, while the containment of electronic modules and ASPW drive are primarily responsible for functionality.

The wheel is the most important design of the entire vessel. We used the ASPW wheel so that the robot can smoothly move in aquatic and land environment without extra transitions. ASPW wheels are mainly composed of paddles, a cover, universal joints, shafts and two gear sets (As shown in Figure 5). The ASPW includes six 3D printed paddles. The number of paddles is sufficient in supporting the balance of the robot on the ground without adding extra load on the gear set. The gear set consists of planetary gears. There is a total of 6 gears P1 running around the gear S1 in the center. Part 2 includes three external gears. Gear M rotates the ASPW by receiving power from a set of gear system connected to the motor.

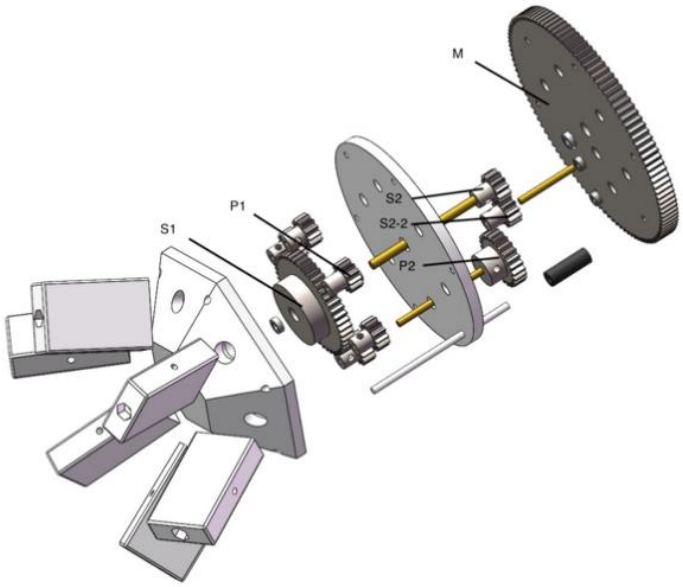

Figure 5. Structure of paddle wheel.

The main shaft in the middle is fixed to the hull. When gear M receives power from the motor, all parts of the ASPW rotate together as they are constrained by the beam and bracket. Since the gear ratio of the external gears S2, S2-2, and P2 of part 2 is 1:1:2, when S2 and S2-2 rotate once, P2 rotates half the time. This makes the top and bottom paddles perpendicular to each other when the paddles rotate. The planetary gear system S1 and P1 determine the angle that the paddles form with each other. The number of gear teeth of S1 is 48, and that of P1 is 12. By designing the number of gear teeth to be a multiple of 6, P1 can maintain a constant distance from each other when rotating. The paddles rotate 90° for every 180° the ASPW wheel rotates, allowing the bottom paddle to be vertical and the top wheels to horizontal.

There is a total of 6 planetary gears P1 running around the central sun gear S1. The universal joint is connected to the shafts that go through P1, so that when P1 rotates, the paddle can rotate together. The bracket is fixed with universal joints, and the cover is fixed with six brackets. The second part includes three external gears. Gear M rotates ASPW by receiving power from the motor.

Cover (Figure 6a): The bottom of the cover is a 52mm hexagon, the top is a 23mm hexagon, the overall height is 30mm, the diameter of the hole in the center is 7mm, the diameter on the hexagonal corners is 3.2 (six), and the diameter of the universal joint hole is 9.5mm.

Paddle (Figure 6b): The paddle is a rectangular prism of 50mm by 30mm by 12mm, with a 3mm diameter hole in the middle and a hexagon with a side length of 4 at the bottom.

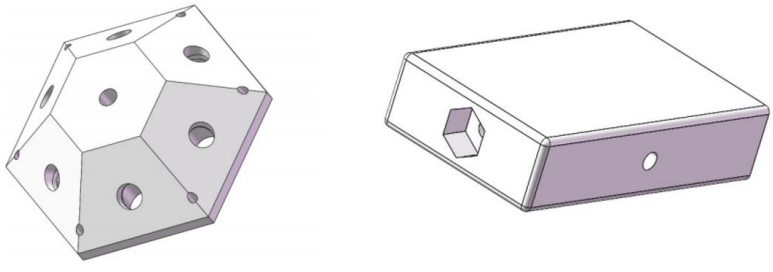

(a) (b)

Figure 6. Cover and paddle module.

S2-2, P1

The number of teeth is 12 with a module of 1. The gear has a thickness of 6mm, with an 8mm high cylinder. The diameter of the cylinder is 4mm, with a 3mm wide shaft whole in the center and on the side (Figure 7).

Figure 7. 12-tooth gear.

S2

All is the same with S2-2 except the central shaft whole is 4mm, as the gear rotates at a different rate with the main shaft.

P2

The number of teeth is 24 with module of 1. The gear has a thickness of 6mm, with an 8 mm high cylinder. The diameter of the cylinder is 7.5mm, with a 3mm wide shaft whole in the center and on the side (Figure 8).

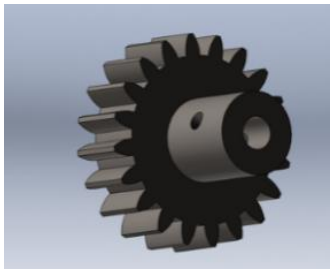

Figure 8. 24-tooth gear.

S1

The number of teeth is 48 with module of 1. The gear has a thickness of 6mm, with an 8 mm high cylinder. The diameter of the cylinder is 15mm, with a 7mm wide shaft whole in the center and 3mm wide hole on the side (Figure 9).

Figure 9. 48-tooth gear.

M

The number of teeth is 110 with module of 1. The gear has a thickness of 6mm. The central shaft whole is 7mm, surrounded by six 6mm whole. In between one of the whole and the central whole is another 6mm whole. On outside there are six 3mm whole (Figure 10).

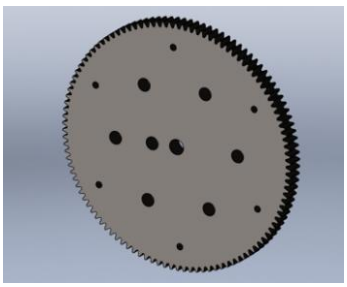

Figure 10. 110-tooth gear.

Ship hull: The overall size of the hull is 220mmX212mmX110mm (Figure 11). The thickness of the hull is 6mm, which meets the strength requirements. There are two fixed brackets for stepper motors inside, with an angle of 135 degrees from the horizontal direction. Equipped with 4 bolt fixing holes. There are fixing holes for the gear shaft on both sides, and 8 support frames at the bottom, each with two fixing holes.

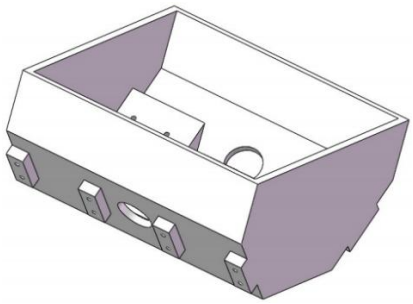

Figure 11. Ship Hull.

Motor bracket: 53mm x 50mm x 50mm, 3mm thick, with a 22mm wide whole in the center (Figure 12).

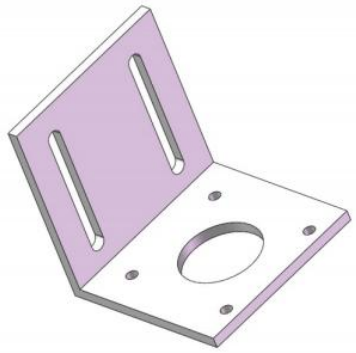

Figure 12. Motor bracket.

2.1.2. Version 2

After designing the first generation of the robot, the basic effect of the impeller was achieved. However, it was later discovered that the gear transmission structure of the impeller structure itself was too large, which produced too much resistance, and the transmission was too complicated, resulting in a high failure rate. Therefore, in order to solve this series of problems, we tried to use the connecting rod structure to simplify the complex transmission of the gears. Secondly, we designed a wedge-shaped hull structure to reduce the resistance caused by the vertical forward shell (Figure 13).

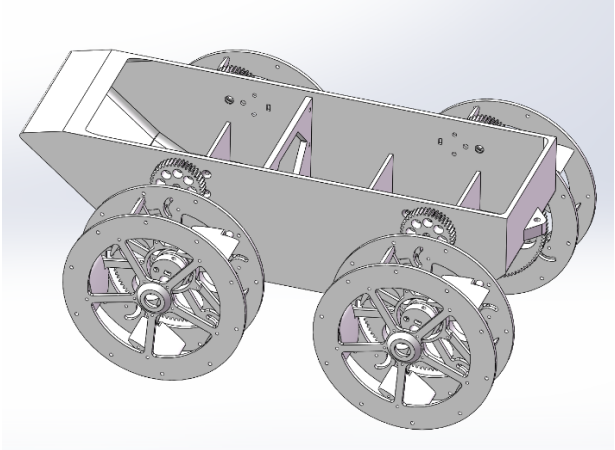

Figure 13. The second-generation version of the impeller structure.

The cycloidal impeller structure is achieved by driving the circumferential blades through the connecting rod connected to the middle eccentric wheel (Figure 14). During the rotation of the wheel, due to the push of the eccentric wheel, the blades will swing regularly, thereby generating thrust.

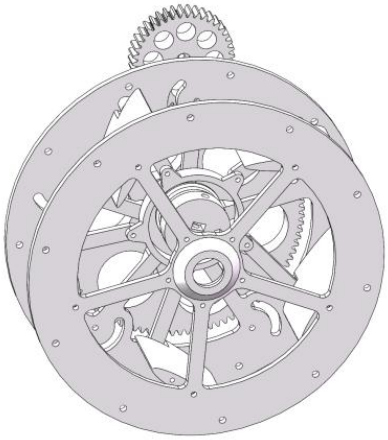

Figure 14. Cycloidal impeller structure.

The new version of the hull structure is made of integrated 3D printing, and each wheel is driven by a separate motor (Figure 15). The motor shaft is installed at a higher position on the hull to prevent water from entering the cabin from the motor shaft. In addition, there are multiple baffles in the cabin, which can improve the overall waterproof performance of the robot.

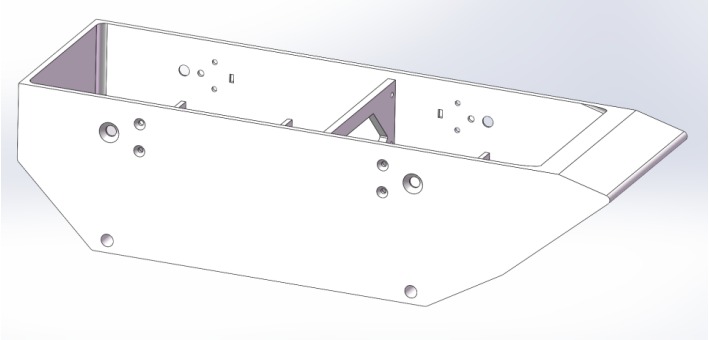

Figure 15. New hull structure.

2.2. Electronical Design

2.2.1. Version 1

Due to the multiple mechanical modules, the electrical component of the robot is limited to 2 motors, an Arduino chip, Bluetooth transmitter, and a battery. The two motors, secured to two extensions on the hull of the robot, each provides propulsion for two wheels on the same side. The motor is connected to a self-designed PBC board (Figure 16). The board is designed to lead the pins of Arduino Nano to other section of the board, making it earlier and clearer when wiring. By adding extra CVV and GND slots, the board allows additional modules such as camera or sensors to be installed. For power, the robot uses a rechargeable 3 cell 18650 lithium batterie. The battery outputs a 12V current. Arduino Nano requires 5V current to function, which is different from the 12V produced by the battery. Therefore, the PBC board has pins for 12V-5V voltage regulator to conduct the 12V from the battery to 5V. To achieve remote control, we used a PS2 controller. The PS2 controller include a Bluetooth module for transmitting signal. The PBC board has a set of pins to connect the module to Arduino Nano.

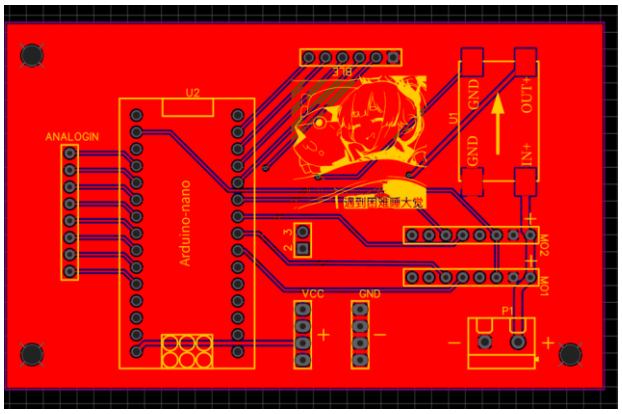

Figure 16. PBC board.

Figure 17. Arduino NANO board.

Arduino NANO is a popular open-source microcontroller board based on the ATmega328P microcontroller (Figure 17). It is widely used in robotics, DIY electronics, and educational projects due to its versatility and ease of use. The board features 14 digital input/output pins (6 of which can be used for PWM output), 6 analog input pins, a 16 MHz crystal oscillator, a USB connection, a power jack, an ICSP header, and a reset button. It operates at 5V and can be powered through a USB cable, an external power supply, or batteries. Arduino Uno supports various programming languages, including C and Arduino-specific language, and can be programmed using the Arduino IDE.

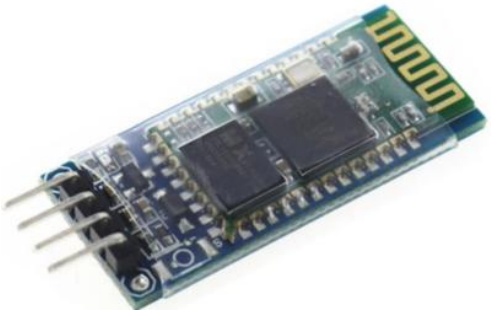

Figure 18. BT-18.

A 5V voltage regulator module is essential for providing stable power to electronic components that require a 5V supply. These modules typically use DC-DC conversion technology to efficiently step-down higher input voltages (e.g., from a 12V battery) to a stable 5V output (Figure 19). They are crucial in robotics and electronics projects to ensure that components such as microcontrollers, sensors, and actuators receive the correct voltage levels to function properly.

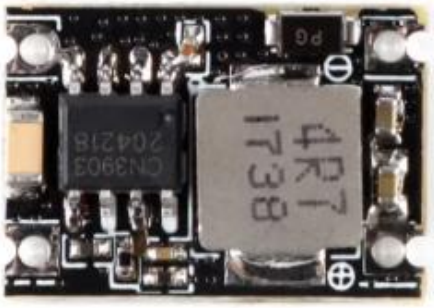

Figure 19. 5V DC-DC module.

The BT18 is a dual-mode Bluetooth module based on the Bluetooth 4.2 standard (Figure 18). It supports both Bluetooth Classic (SPP) and Bluetooth Low Energy (BLE) protocols, making it suitable for a wide range of wireless communication applications. The module features a UART interface for data transmission, a communication range of up to 40 meters in open environments, and low power consumption.

Figure 20. S2 remote controller.

The PS2 remote controller is a versatile input device originally designed for gaming but widely adapted for robotics and DIY projects (Figure 20). It typically features multiple buttons and joysticks that can be mapped to control various functions in a robot or electronic system. The controller communicates with the host device using a standard PS2 protocol, which can be easily interfaced with microcontrollers like Arduino.

2.2.2. Version 2

The improved second-generation version abandons the dual stepper motor structure of the first generation and directly uses four reduction motors as power, ensuring the reliability of the robot while reducing the overall weight of the robot.

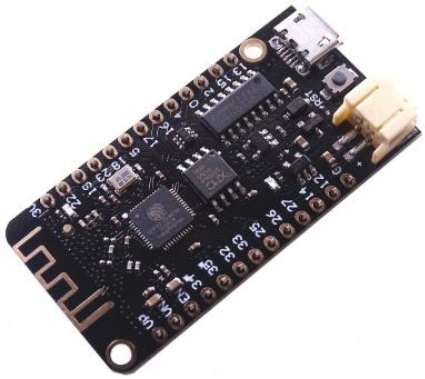

Figure 21. ESP32 board.

The ESP32 is a highly versatile and powerful microcontroller module designed for Wi-Fi and Bluetooth-enabled IoT applications (Figure 21). It features a dual-core processor, integrated Wi-Fi, and Bluetooth capabilities, making it suitable for a wide range of applications, from simple automation tasks to complex IoT projects. The module supports multiple programming languages, including C, Python, and the Arduino framework, and can be programmed using the ESP-IDF or Arduino IDE. Replacing it with ESP32 here can simplify the electronic module.

Figure 22. A4950.

The A4950 is a full-bridge DMOS PWM motor driver designed for controlling DC motors (Figure 22). It can handle peak output currents up to ±3.5 A and operate at voltages up to 40 V. The module uses low-RDS (on) N-channel DMOS drivers with internal synchronous rectification to reduce power dissipation during PWM operation.

2.3. Code

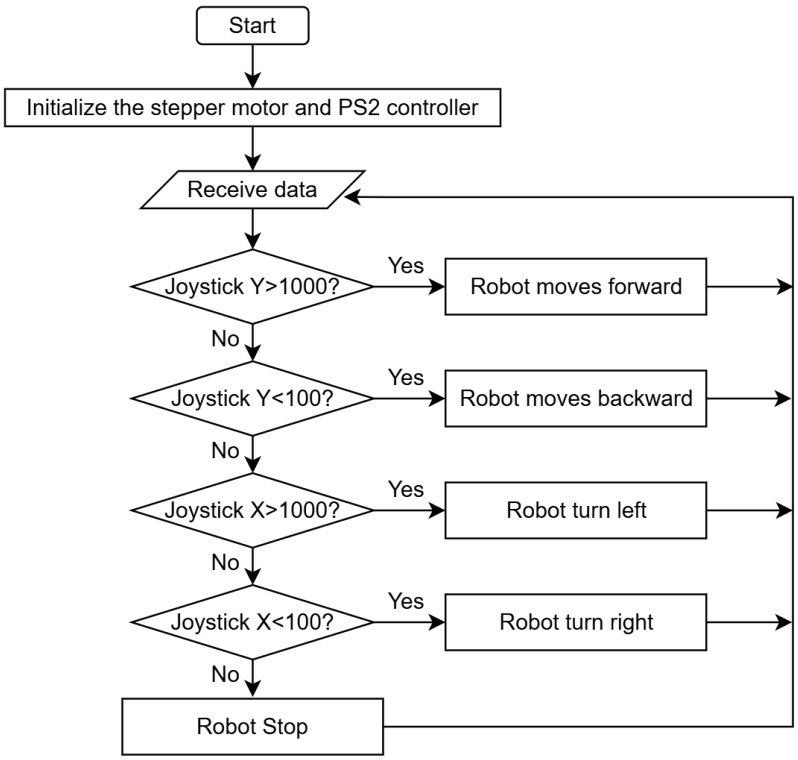

Figure 23. Program flowchart.

The flowchart outlines (Figure 23) the process for controlling a robot's movements using a PS2 controller. The process begins with the initialization of the stepper motor and PS2 controller. Once initialized, the robot enters a loop where it continuously receives data from the PS2 controller.

The control logic is based on the joystick's Y and X-axis values:

- If the joystick's Y-axis value exceeds 1000, the robot moves forward.
- If the Y-axis value is less than 100, the robot moves backward.
- If the X-axis value exceeds 1000, the robot turns left.
- If the X-axis value is less than 100, the robot turns right.
- If none of these conditions are met, the robot stops.

This loop continues, allowing for real-time control of the robot's movements based on the joystick's input.

3. Experiment

3.1. Version 1

3.1.1. Land experiment

Experimental objective: This experiment aims to test the stable walking ability of a self-made device, by simulating the walking state at different time points (1 second, 2 seconds, 3 seconds, 4 seconds), and observing the stability and adaptability of the device during the walking process (Figure 24).

Experimental method: Walk on a flat ground through a control device and capture its walking posture at different time points to evaluate its stability and gait coherence.

Experimental results: From the picture, it can be seen that the device can maintain a stable walking posture within 1 second to 4 seconds. In the initial stage (1 second), the gait of the device started smoothly without any significant shaking or imbalance. As time goes by (2 seconds to 4 seconds), the device continues to maintain a stable pace, demonstrating good balance control ability.

Stability analysis: The stability of the device is due to its design, including a low center of gravity and a wide support foundation, which helps maintain balance during walking. In addition, the joint design of the device allows for necessary adjustments during walking to accommodate small changes in the ground.

Gait coherence: In the experiment, the device exhibited a coherent gait, with each step closely following the previous one without any stagnant or uncoordinated movements. This indicates that the control system of the device can effectively coordinate the movements of various joints and achieve smooth walking.

Experimental conclusion: This experiment successfully verified the stable walking ability of the self-made device. The device demonstrated good stability and gait coherence during the testing process, enabling smooth walking on flat surfaces. Future work can focus on improving the walking ability of the device on more complex terrains, as well as further optimizing its control system to achieve more efficient and flexible walking movements.

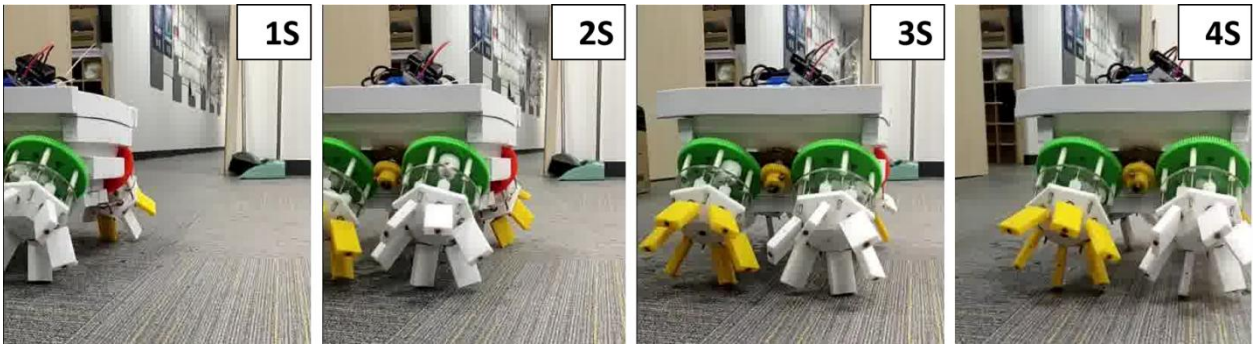

Figure 24. Land walking test.

Experimental objective: This experiment aims to test the ability of a self-made device to climb over large obstacles. By simulating the crossing process at different time points (1 second to 8 seconds), observe the adaptability and stability of the device when facing obstacles (Figure 25).

Experimental method: The device is designed to recognize and climb over transparent plastic obstacles placed in the path. The experiment involves setting obstacles along the path of the device and recording the entire process of overcoming them.

Experimental results: From the picture, it can be seen that the device successfully approached and prepared to climb over obstacles within 1 second to 4 seconds. Within 5 to 6 seconds, the device begins to attempt to climb over obstacles, demonstrating the flexibility of its structure and the accuracy of its control system. At 7 to 8 seconds, the device has successfully climbed over the obstacle and continued to move forward.

Analysis of Climbing Ability: The climbing ability of the device benefits from its design, including adjustable leg joints and a stable torso, which helps maintain balance during the climbing process. In addition, the sensor system of the device can effectively identify obstacles and adjust strategies to successfully climb over them.

Stability analysis: During the process of overcoming obstacles, the device exhibits good stability. Despite some swaying during the climb, the device was able to quickly adjust and maintain balance, indicating that its control system has high robustness.

Experimental conclusion: This experiment successfully verified the ability of the self-made device to climb over large obstacles. The device demonstrated good adaptability and stability during the testing process, effectively identifying and overcoming obstacles. Future work can focus on improving the navigation capability of the device in more complex environments, as well as further optimizing its control system to achieve more efficient and flexible climbing actions.

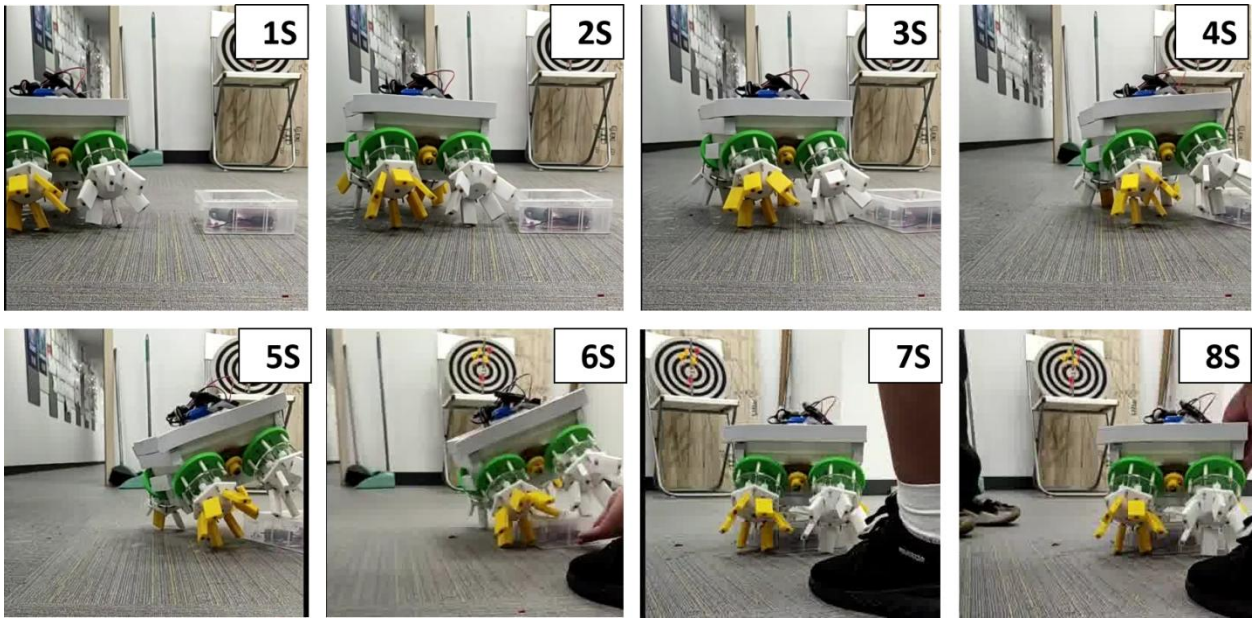

Figure 25. Land obstacle test.

Experimental objective: This experiment aims to test the ability of a self-made device to climb over small sheet-like obstacles. By simulating the crossing process at different time points (1 second to 8 seconds), observe the adaptability and stability of the device when facing small obstacles (Figure 26).

Experimental method: The device is designed to recognize and overcome small sheet-like obstacles placed in the path. The experiment involves setting obstacles along the path of the device and recording the entire process of overcoming them.

Experimental results: From the picture, it can be seen that the device successfully approached and prepared to climb over obstacles within 1 second to 4 seconds. Within 5 to 6 seconds, the device begins to attempt to climb over obstacles, demonstrating the flexibility of its structure and the accuracy of its control system. At 7 to 8 seconds, the device has successfully climbed over the obstacle and continued to move forward.

Analysis of Climbing Ability: The climbing ability of the device benefits from its design, including adjustable leg joints and a stable torso, which helps maintain balance during the climbing process. In addition, the sensor system of the device can effectively identify obstacles and adjust strategies to successfully climb over them.

Stability analysis: During the process of overcoming obstacles, the device exhibits good stability. Despite some swaying during the climb, the device was able to quickly adjust and maintain balance, indicating that its control system has high robustness.

Experimental conclusion: This experiment successfully verified the ability of the self-made device to climb over small sheet-like obstacles. The device demonstrated good adaptability and stability during the testing process, effectively identifying and overcoming obstacles. Future work can focus on improving the navigation capability of the device in more complex environments, as well as further optimizing its control system to achieve more efficient and flexible climbing actions.

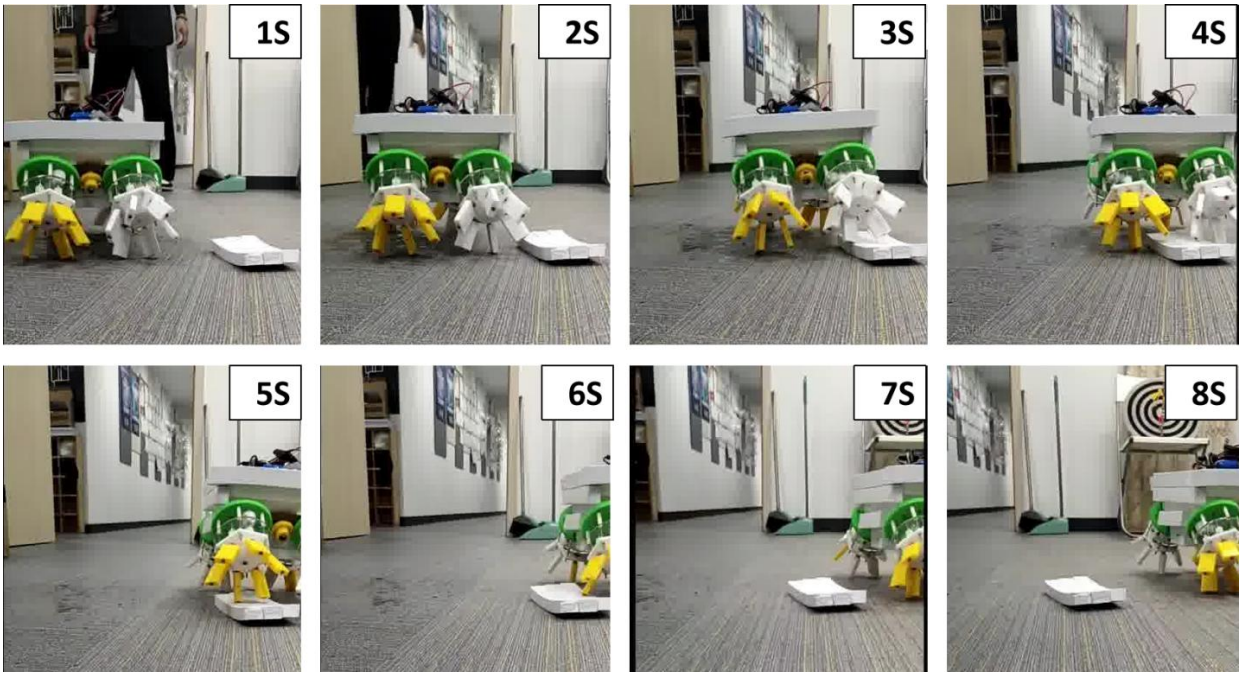

Figure 26. Land obstacle test 2.

3.2. Aquatic experiment

Experimental objective: This experiment aims to test the free movement ability of a self-made device in water, in order to verify its waterproof performance and stability of movement in water (Figure 27).

Experimental method: The device is placed in a container filled with water and its behavior is observed at different time points (1 second to 9 seconds) to evaluate its mobility and stability in water.

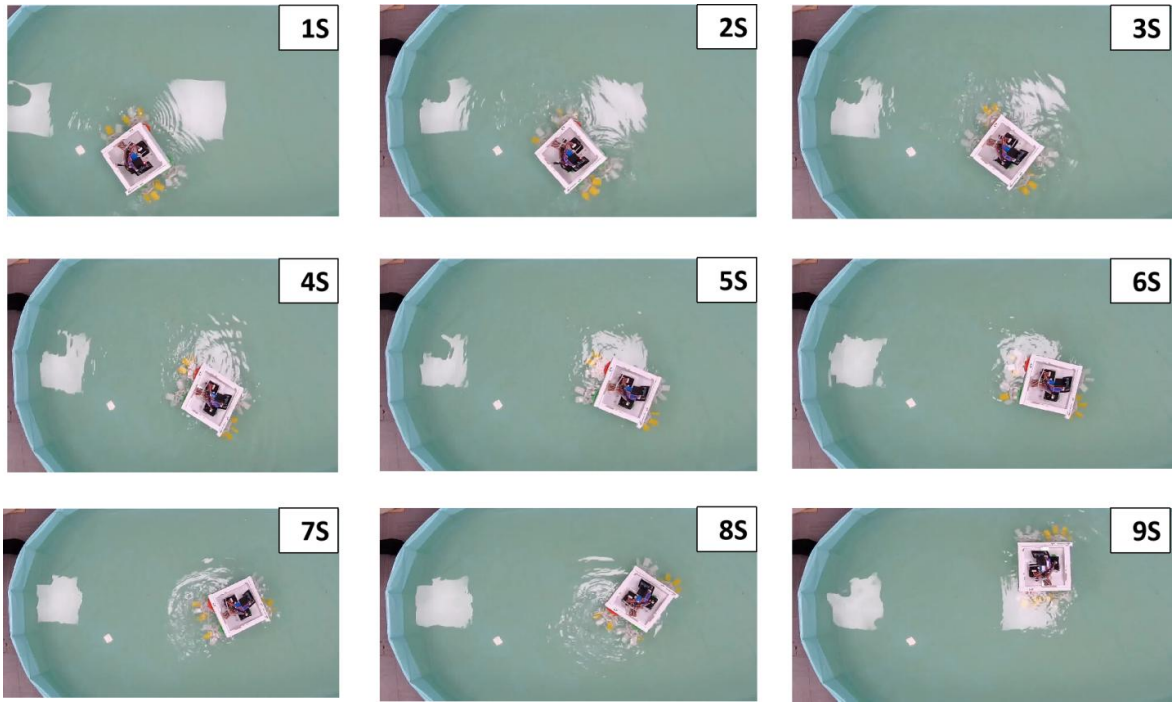

Figure 27. Aquatic experiment.

Experimental results: From the picture, it can be seen that the device successfully moved freely in water within 1 second to 9 seconds. In the initial stage (1 second to 3 seconds), the device starts to start and gradually gains power in the water. During the period of 4 to 6 seconds, the device's movement in water became more stable, demonstrating the effectiveness of its waterproof design. By

7 to 9 seconds, the device is capable of performing complex movements in the water, including steering and depth adjustment.

Analysis of in water mobility: The device's underwater mobility benefits from its design, including waterproof electronic components and a propulsion system capable of generating thrust underwater. In addition, the buoyancy control and balance system of the device also helps it maintain stability in water.

Stability analysis: During underwater operations, the device exhibits good stability. Despite the influence of buoyancy and water flow in underwater environments, the device is able to quickly adjust and maintain balance, indicating that its control system has high adaptability.

Experimental conclusion: This experiment successfully verified the free movement ability of the self-made device in water. The device demonstrated good waterproof performance and water stability during the testing process, and was able to effectively move and turn in water. Future work can focus on improving the energy efficiency of the device, optimizing its propulsion system, and further enhancing its navigation and operational capabilities in complex underwater environments.

3.3. Version 2

Experiment Purpose: To investigate the maximum climbing angle with a serrated wheel (Figure 28).

Experimental Steps:

1. Use screws in conjunction with a wooden board structure to build a fixed rough surface structure.
2. Use cardboard boxes to prop up the wooden board and combine it with an angle measuring device to indicate the inclination angle of the board.
3. Place a steel ruler as a reference and secure the camera stand to capture the climbing process.
4. Sequentially capture the climbing scenarios at different angles.
5. Use Tracker software for velocity analysis.

Figure 28. Experimental climbing scenarios at different angles.

Experimental Results:

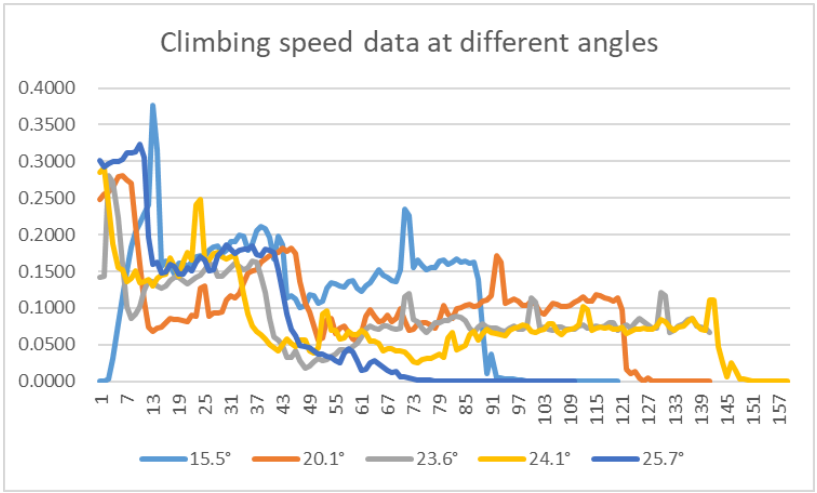

Figure 29. Velocity data during the climbing process.

Experimental Analysis:

The average speed of the robot decreases with increasing inclination angle (Figure 29). With the addition of a serrated wheel structure, the maximum climbing angle can reach 24 degrees. As the

angle increases further, slipping tends to occur. In the future, it is possible to test with a higher-torque motor or larger serrations to enhance the robot's climbing capability on slopes.

4. Summary and outlook

The project basically achieved the expected design goals through the physical construction of two versions. The water and land tests of this four-wheeled amphibious robot were completed, and the slope climbing test was added to the second-generation version, which is more suitable for rescue scenarios such as trapped reefs. It is a good solution to the reef area that the rescue ship cannot approach.

In the future, the robot can be deployed on the beach, and with the intelligent monitoring system, it can complete intelligent rescue on the sea surface, greatly reducing the rescue preparation time and avoiding additional damage during the rescue process.

References

[1] Rafeeq M, Toha S F, Ahmad S, et al. Locomotion strategies for amphibious robots-a review. IEEE Access, 2021, 9: 26323 - 26342.

[2] Saranli U, Buehler M, Koditschek D E. RHex: A simple and highly mobile hexapod robot. The International Journal of Robotics Research, 2001, 20 (7): 616 - 631.

[3] Liang X, Xu M, Xu L, et al. The AmphiHex: A novel amphibious robot with transformable leg-flipper composite propulsion mechanism. 2012 IEEE/RSJ International Conference on Intelligent Robots and Systems, 2012: 3667 - 3672.

[4] Vogel A R, Kaipa K N, Krummel G M, et al. Design of a compliance assisted quadrupedal amphibious robot. 2014 IEEE International Conference on Robotics and Automation (ICRA), 2014: 2378 - 2383.

[5] Park H S, Sitti M. Compliant footpad design analysis for a bio-inspired quadruped amphibious robot. 2009 IEEE/RSJ International Conference on Intelligent Robots and Systems, 2009: 645 - 651.

[6] Kashem S B A, Jawed S, Ahmed J, et al. Design and implementation of a quadruped amphibious robot using duck feet. Robotics, 2019, 8 (3): 77.

[7] Shim H, Yoo S Y, Kang H, et al. Development of arm and leg for seabed walking robot CRABSTER200. Ocean Engineering, 2016, 116: 55 - 67.

[8] Ayers J. Underwater walking. Arthropod structure & development, 2004, 33 (3): 347 - 360.

[9] Dudek G, Jenkin M, Prahacs C, et al. A visually guided swimming robot. 2005 IEEE/RSJ International Conference on Intelligent Robots and Systems, 2005: 3604 - 3609.

[10] Rodríguez-Martínez D, Van Winnendael M, Yoshida K. High-speed mobility on planetary surfaces: A technical review. Journal of Field Robotics, 2019, 36 (8): 1436 - 1455.